Peer-reviewed version available at *Materials* **2019**, *12*, 3067; doi:10.3390/ma12193067

Article

Corrosion Inhibition Mechanism and Efficiency Differentiation of Dihydroxybenzene Isomers towards Aluminium Alloy 5754 in Alkaline Media

Jacek Ryl [1]*, Mateusz Brodowski [1,2], Marcin Kowalski [1,2], Wiktoria Lipinska [1,3], Pawel Niedzialkowski [4] and Joanna Wysocka [1]

[1] Faculty of Chemistry, Gdansk University of Technology, Narutowicza 11/12, 80-233 Gdansk, Poland
[2] Faculty of Mechanical Engineering, Gdansk University of Technology, Narutowicza 11/12, 80-233 Gdansk, Poland
[3] Centre for Plasma and Laser Engineering, The Szewalski Institute of Fluid-Flow Machinery, Polish Academy of Sciences, Fiszera 14, 80-231 Gdansk, Poland
[4] Faculty of Chemistry, University of Gdansk, Wita Stwosza 63, 80-308 Gdansk, Poland
* Corresponding author: jacek.ryl@pg.edu.pl; Phone number: +48 58 347 1092 (Poland)

Abstract:

Selection of efficient corrosion inhibitors requires detailed knowledge regarding interaction mechanism, which depends on the type and amount of functional groups within the inhibitor molecule. Position of functional groups between different isomers is often overlooked but not less important since factors like steric hinderance may significantly affect the adsorption mechanism.

In this study we have presented how different dihydroxybenzene isomers interact with aluminium alloy 5754 surface, reducing its corrosion rate in bicarbonate buffer (pH = 11). We have shown the highest inhibition efficiency among tested compounds belongs to catechol at 10 mM concentration, although differences were moderate. Utilization of novel impedance approach to adsorption isotherm determination allowed to confirm that while resorcinol chemisorbs on aluminium surface, catechol and quinol follows ligand exchange model of adsorption. Unlike catechol and quinol, the protection mechanism of resorcinol is bound to interaction with insoluble aluminium corrosion products layer and was only found efficient at concentration of 100 mM (98.7%). The aforementioned studies were confirmed with Scanning Electron Microscopy and X-ray Photoelectron Spectroscopy analyses.

There is a significant increase of the corrosion resistance offered by catechol at 10 mM after 24 h exposure in electrolyte: from 63 to 98%, with only negligible changes in inhibitor efficiency observed for resorcinol at the same time. However, in the case of resorcinol a change in electrolyte color was observed. We have revealed that the differentiating factor is the keto-enol tautomerism. The NMR studies of resorcinol indicate the keto form in structure in presence of NaOH, while the chemical structure of catechol does not change significantly in alkaline environment.

Keywords: aluminium alloy, corrosion inhibitor, alkaline environment, impedance analysis, adsorption, dihydroxybenzene

---

1. Introduction

Aluminium is the most widely spread metallic element on Earth **[1]**, owing unique physic-chemical properties, such as: low weight, high thermal and electrical conductivity, high linear expansion coefficient and good corrosion resistance. It is non-magnetic, non-toxic and may be a subject repeatable recycling **[2]**. Aluminium and its alloys have been used in almost all industries,

Peer-reviewed version available at Materials 2019, 12, 3067; doi:10.3390/ma12193067

in particular in mechanical engineering, defense industry, aviation, shipbuilding, food and chemical industries and many others. It is a strategic resource whose consumption is a measure of countries development and industrialization level. Over the past 50 years, the world production of aluminium has been constantly increasing, with the highest leap occurring in this millennium. Limited access to bauxite ores and their gradual depletion are the main obstacles in further development of aluminium industry. Constantly growing demand and utilization of aluminium requires more effective methods for its recycling or protection.

Aluminium and its alloys belong to the group of passivating metals, next to titanium, chromium and high-alloy steels. Spontaneously formed native oxide layer on aluminium surface is build primarily of aluminium oxide Al_2O_3. The layer is thermodynamically stable in the pH range between 4 and 9, where aluminium possess the highest corrosion resistance. On the other hand, the passive layer is not thermodynamically stable in alkaline and acidic media. In the presence of hydroxyl ions aluminium undergoes oxidation to form $Al(OH)_4^-$, according to the mechanism proposed by Macdonald **[3]**. Other researchers shown that direct dissolution of aluminium is impossible and requires formation of aluminium hydroxides $Al(OH)_3$ intermediates **[4–6]**, which may be simplified to the form of eqs. (1-3):

$$Al \longrightarrow Al^{3+} + 3e^- \quad (1)$$

$$Al^{3+} + 3OH^- \longrightarrow Al(OH)_3 \quad (2)$$

$$Al(OH)_3\downarrow + OH^- \longrightarrow Al(OH)_4^- \quad (3)$$

The anodic dissolution is accompanied by cathodic process of water electrolysis with hydrogen generation, according to eq. (4):

$$2H_2O + 2e^- \longrightarrow H_2\uparrow + 2OH^- \quad (4)$$

The problem of aluminium corrosion in the alkaline media occurs in numerous practical cases, starting from its possible application as an anode material in energy storage devices, pre-treatment processes before the anodization or for esthetical purposes, up to alkaline character of various cleaning agents used on working elements and constructions **[7–10]**. One of the most often utilized methods to lower the corrosion rate of aluminium in these environments is application of corrosion inhibitors.

Various organic inhibitors were reported as efficient corrosion inhibitors of aluminium and its alloys. Their inhibition effect depends on the molecule structure, functional groups being electron donors or acceptors and the amount of such groups per molecule **[11,12]**. It is worth to point out that the most effective inhibitors are based on molecules containing heteroatoms such as: oxygen, nitrogen, phosphorous, sulphur and aromatic rings **[13,14]**. Carboxylic acids in particular have been shown as highly efficient corrosion inhibitors of aluminium and its alloys in aqueous alkaline environments **[15–18]**. Studies carried out on maleic, malic, succinic, tartaric, citric and tricarballylic acids revealed changes in corrosion efficiency with the increased amount of -COOH groups and decreased amount of –OH groups within inhibitor molecule **[16]**. Similar reports involved restriction of aluminium corrosion in alkaline media by polyacrylic acids, where studies shown increase of inhibition efficiency with the increase of molecular weight of inhibitor molecule **[19]**. Compounds containing nitrogen and/or sulphur are also proved as efficient corrosion inhibitors, an example of which may be studies on 3-methyl-4-amino-5-mercapto-1,2,4-triazole (MAMT). Inhibitor molecules adsorption on protected metal surface occurs through amine and thiol functional groups **[20]**.

Lashgari and Malek proved that phenol is a highly efficient corrosion inhibitor of aluminium **[21]**. Phenols are deprotonated in alkaline environments and transformed into inhibitory active forms of phenoxide and phenolate. Similar conclusions, based on theoretical studies, were later on drawn for p-phenol derivatives, where the author confirmed that the mechanism of inhibition relies on a complicated cycle of protonation/deprotonation of inhibitor molecules in the inner area of the electrical double layer **[22]**. The mentioned above process leads to local neutralization of corrosive

Peer-reviewed version available at *Materials* **2019**, *12*, 3067; doi:10.3390/ma12193067

factors and their electrostatic repulsion in the vicinity of active metal surface. Corrosion inhibition efficiency of p-phenol derivatives depends on a number of factors, including: electron density on oxygen and hydrogen atoms in hydroxyl group, charge transfer, the energy of interaction, molecular activity, electric dipole moment and Gibbs free energy of the dissolution process.

Increasing attention of corrosion scientists is nowadays focused on application of corrosion inhibitors of natural origin, obtained in accordance with the principles of green chemistry. Green corrosion inhibitors in the form of plant extracts are eco-friendly, non-toxic and biodegradable in neutral environments **[23–31]**. For example, *Phyllanthus amarus* leaf extract offers nearly 75% efficiency in 2M NaOH solution **[32]**. The extract contains alkanoids, cyanogenic glycosides, flavonoids, carbohydrates, sugar, proteins, triterpenoids and steroids. Functional groups -OH, $-NH_2$, -SH, present in mentioned above compounds and π-bonds are most likely responsible for inhibition efficiency of *Phyllanthus amarus.* On the other hand, *Piper longum* seed extract, with 94% efficiency at concentration of 0.4 $g \cdot L^{-1}$ in 1 M NaOH, contains piperine, piperlongumine, piplartine, piperlonguminine, piperundecalidinine and pipernonaline **[33]**. The high inhibition efficiency was explained with presence of N-heteroatoms and π-electrons in aromatic rings. The 92% inhibition efficiency of *Gossypium hirsutum* extract in 2 M NaOH most likely originates from presence of O, N or S in amino acids such as: cysteine, lysine, methionine, phenylalanine, arginine, threonine, tyrosine, tryptophan, valine, but also polyphenolic aldehyde and tannins **[34]**. Authors also observed that higher concentration of active substances in present in leafs rather than seeds of *Gossypium hirsutum.*

Green corrosion inhibitors in the form of extracts from natural products are characterized by a large amount of chemical compounds. In such a complex mixture of potential inhibitory compounds it is particularly important to perform phytochemical studies in order to determine the active compounds and their mechanism of interaction, which in many cases appears to be incredibly difficult task. Therefore, in order to avoid blind-picking during selection of natural extracts containing potentially efficient inhibitor compounds one must get to know in details the mechanism of interaction of various types of functional groups with protected metal surface as well as how its modified by other aspects of the molecule structure. A valuable approach towards more effective determination of the active inhibitory compounds may be found in designing the extraction process. Differentiation of the type of solvents or extraction conditions leads to selective extraction of certain groups of compounds. Ryl et al. **[35]** shown that bee pollen extracts prepared through extraction in different solvents results in different corrosion inhibition efficiency towards AA5754 in bicarbonate buffer at pH = 11. It has been proven that these differences are caused by varying content of carboxylic acids and phospholipids, which acted as inhibitory active substances in bee pollen extracts.

A certain group of phenol derivatives exhibits very high corrosion inhibition efficiency towards aluminium and its alloys. This group includes catechol, cresol, chlorophenol, resorcinol, nitrophenol and aminophenol **[36,37]**. Talati and Modi **[36]** suggested that $-OCH_3$, $-NH_2$ and $-CH_2CHCH_3$ functional groups lower the inhibition efficiency of phenol, while -OH, -Cl, $-NO_2$ increase it. Furthermore, they suggested three different adsorption mechanisms, namely: through electrostatic forces, formation of chelating agents with aluminium ions or covalent bond formation. Authors also observed that the inhibition efficiency decreases with the increase of electrolyte alkalinity. The synergistic interaction of resorcinol with Zn^{2+} ions was further studied by Lakshmi et al. **[37]**, which revealed significant increase of corrosion inhibition efficiency of aluminium. However, all the aforementioned studies were carried out using gravimetric method, introducing significant uncertainty of the measurements. The formation of the insoluble corrosion products layer on aluminium surface hinders specific determination of weight loss of the analyzed samples.

Not only the type and the number of active functional groups but also their position in the molecule structure may have a significant influence on corrosion inhibition efficiency. The chemical structure of isomer molecules affects modification of their physic-chemical properties such as solubility, while steric hinderance may influence both kinetics and mechanism of the adsorption

Peer-reviewed version available at Materials 2019, 12, 3067; doi:10.3390/ma12193067

process. This subject was not given sufficient attention in the corrosion research, however several available reports prove the importance of substituents position in the molecule **[38–40]**. Fouda and Elasmy **[38]** presented their studies on phenylthiosemicarbazide derivatives as aluminium corrosion inhibitors in 2M NaOH, with efficiency ranging between 75.0 and 98.5%, depending on the derivative. Hassan et al. **[39]** confirmed that the efficiency of aromatic carboxylic acids depends on the number and position of carboxylic groups and presence of other substituents in aromatic ring. The increasing corrosion efficiency was as follows: benzamide < benzaldehyde < acetophenone < benzoic acid < benzophenone (99.99% efficiency).

The electrochemical impedance studies on thiosemicarbazone interaction with aluminium alloys in 1 M HNO_3 revealed almost 20% higher inhibition efficiency offered by para-substituted compounds in comparison to ortho-substituted ones **[41]**. There is no general relationship through. The search for corrosion inhibitors of mild steel in 1 M HCl revealed that ortho-nitroaniline and ortho-methyloaniline show higher corrosion inhibition efficiency in comparison with both meta- and para-substituents, but in the case of phenlylenediamine meta-substituted functional groups offered the highest efficiency **[42]**. Similar observation was made on aminophenol-N-salicylidene isomers action towards zinc in 0.5 M H_2SO_4 **[43]**.The goal of this work is to evaluate the influence of position of hydroxyl functional groups within dihydroxybenzene molecule on the corrosion inhibition provided by the isomer towards aluminium in alkaline electrolytes. Dihydroxybenzene isomers (catechol, quinol and resorcinol) were utilized, as presence of hydroxyl functional groups is expected to provide reasonable inhibition efficiency in studied electrolytes. In our studies we have implemented newly developed instantaneous impedance tool, i.e. Dynamic Electrochemical Impedance Spectroscopy in galvanostatic mode (g-DEIS), which is capable of accurate and time-efficient determination of the adsorption mechanism differences **[15,16,35]**.

2. Materials and Methods

2.1 Materials

The studied material was aluminium alloy 5754, which had the following alloying additives (in wt.%): Mg 3.6, Fe 0.3, Si 0.3, Cr 0.1, Mn 0.5, Ti 0.1 and Cu 0.1. Cylindrical samples were cut from a rod and subjected to pretreatment procedure in form of grinding and polishing, carried out on Digiprep 251 (Metkon, Turkey) polishing machine. Samples were grinded on a waterproof abrasive papers SiC 600 and 1500, polished with diamond suspensions 6 and 1 μm and mirror finished on 0.05 μm silica. Following polishing, samples were cleaned and degreased in acetone using ultrasonic cleaner. Samples were exposed to corrosion studies with 0.5 cm^2 surface area.

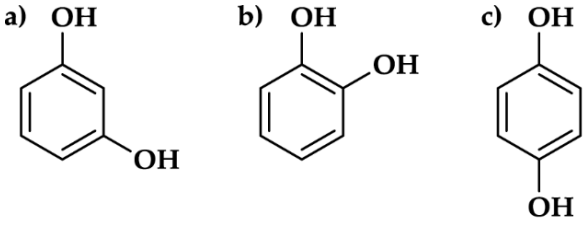

Fig. 1 - The chemical structure of dihydroxybenzene isomers: a) resorcinol; b) catechol; c) quinol.

The primary electrolyte was the bicarbonate buffer solution. The buffer was prepared using 227 cm^3 0.1 M NaOH and 500 cm^3 0.05 M $NaHCO_3$, diluted with deionized water to 1 dm^3 volume. The obtained buffer had pH = 11 and conductivity of 3.8 $mS \cdot cm^{-1}$. All were analytical purity Sigma Aldrich reagents. Three dihydroxybenzene isomers were evaluated, namely: resorcinol, catechol and quinol. Their chemical structures are presented on Fig. 1. The corrosion inhibition efficiency of the aforementioned compounds was investigated at various inhibitor concentrations c_{inh} = 1, 10 and 100 mM as well as with linearly changing inhibitor concentration during g-DEIS studies related with inhibitor injection into the corrosion cell.

Peer-reviewed version available at Materials 2019, 12, 3067; doi:10.3390/ma12193067

2.2 Electrochemical measurements

The electrochemical impedance studies were performed in a three electrode setup. Investigated aluminium alloy 5754 was the working electrode (WE), $Ag|Ag_2O$ was the reference electrode (RE) ($E° = +0.215$ V vs SHE) while Pt mesh served as the counter electrode (CE). The electrolyte volume in the corrosion cell was 10 mL.

Corrosion inhibition efficiency studies were performed by means of classic Electrochemical Impedance Spectroscopy (EIS) and Dynamic Electrochemical Impedance Spectroscopy in galvanostatic mode (g-DEIS) after the initial conditioning for 15 min. EIS was carried out in potentiostatic mode, at open circuit potential (OCP) conditions. The perturbation signal for EIS measurements was applied in the frequency range between 50 kHz and 40 mHz, with 10 points per decade of frequency and amplitude of 15 mV. Multisinusoidal perturbation signal for g-DEIS studies composed of 29 superimposed elementary signal in the frequency range between 4.5 kHz and 1.0 Hz, with 8 points per decade of frequency. Sampling frequency was 128 kHz. The amplitude of perturbation signal was controlled to assure amplitude of response signal doesn't exceed 15 mV. The analysis window for the Short-time Fourier Transformation was 10 s in length. Similar measurement procedure was previously applied in corrosion studies **[15,16,35,44–46]**.

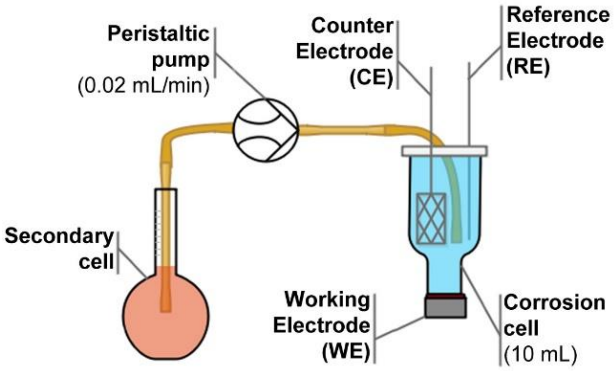

Fig. 2 – Schematic representation of the setup used during electrochemical studies.

In order to build the adsorption isotherm, studied corrosion inhibitor was injected from the secondary cell to the corrosion cell through BQ80S microflow peristaltic pump (Lead Fluid, China). The flow rate was set as 0.02 $mL \cdot min^{-1}$. The concentration of studied inhibitor in the secondary cell was set in a way to assure corrosion inhibitor concentration in the corrosion cell (c_{inh}) equal to 10 mM at the end of 6000 s long experiment. The corrosion cell was thermostated at 25 °C. The electrochemical setup used during all corrosion studies is schematically presented on Fig. 2.

2.3 Equipment

The EIS measurements were carried out using frequency-response-analysis on Gamry Reference 600+ potentiostat (Gamry Instruments, USA). The g-DEIS measurement system consisted of Autolab PGSTAT 302N (Metrohm, Netherlands) galvanostat connected to PXI-4464 measurement card for AC signal generation and PXI-6124 card for AC/DC signal acquisition, both operating in PXIe-1073 chassis (all from National Instruments, USA). The microflow peristaltic pump used was BQ80S (Lead Fluid, China). The thermostat was Corio CD (Julabo GmbH, Germany)

Microscopy analyses of AA5754 corrosion process were performed on Scanning Electron Microscope VP-SEM S-3400 N (Hitachi, Japan), equipped with a tungsten source and operating at 20 kV accelerating voltage. SEM micrographs were done in secondary electron mode.

High-resolution X-Ray Photoelectron Spectroscopy (XPS) analyses were performed on Escalab 250 Xi multispectroscope (ThermoFisher Scientific, USA). The spectroscope is equipped in Al Kα X-ray source with a spot diameter of 250 μm. The measurements were carried out at 20 eV pass energy and 0.1 eV energy step size. The charge compensation was provided by means of low-energy electrons and low-energy Ar+ ions emission from the flood gun.

Nuclear Magnetic Resonance (NMR) spectra were recorded on AVANCE III 500 MHz NanoBay spectrometer (Bruker, USA). Tetramethylsilane (TMS) was used as an internal standard in all the measurements. The 0.5 mL solution containing 80 mM dihydroxybenzene isomer in D_2O was filled with NaOH. The titrated compounds ratio to NaOH was 1:1, 1:5 and 1:10. ^{1}H-NMR and ^{13}C-NMR spectra were recorded. All the measurements were performed after 24 h in 25 °C and in the same volume of solvent.

3. Results and discussion

3.1. Dihydroxybenzene isomers as corrosion inhibitors

The Electrochemical Impedance Spectroscopy (EIS) was used during the preliminary studies to assess the corrosion resistance of the investigated aluminium alloy immersed in alkaline environment with the addition of each dihydroxybenzene isomer. The studied were carried out for three different corrosion inhibitor concentrations c_{inh}, namely: 1, 10 and 100 mM. The impedance spectra presented in the form of Nyquist plot are plotted on Fig. 3. It can be seen by the shape of the impedance semicircles, that studied derivatives offer different level of corrosion protection, however detailed analysis required fitting of the obtained data with electric equivalent circuit (EEC).

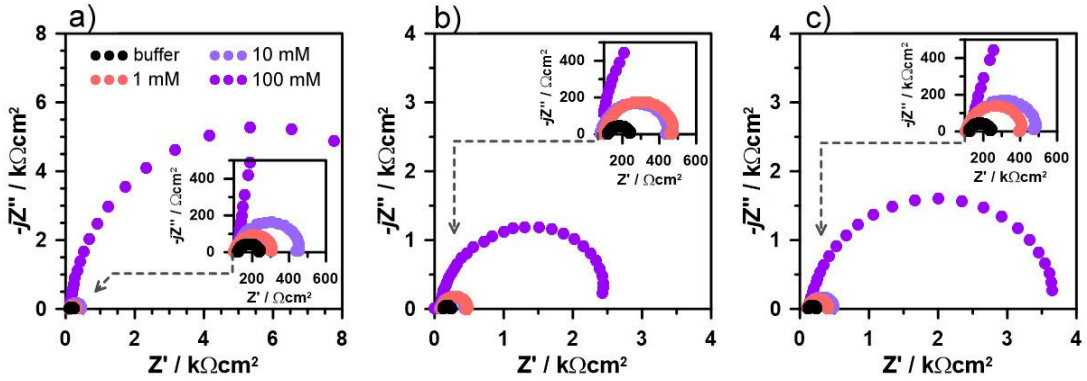

Fig. 3 – EIS impedance spectra recorded for AA5754 exposed to bicarbonate buffer (pH = 11) with addition of studied dihydroxybenzene isomers: a) resorcinol; b) catechol; c) quinol at various concentrations in range 1 – 100 mM.

There is only one clear time constant present on the obtained impedance spectra, suggesting that the charge transfer through the electrode interface and through the adsorbed inhibitor layer are characterized with similar relaxation times. Authors decided to apply a simple form of Randles electric equivalent circuit (EEC) due to prominence of one time constant on the impedance spectra in the applied frequency range. The one and only alteration was to replace capacitance parameter with constant phase element (CPE) in order to properly consider investigated electrode surface heterogeneity, originating from alloy microstructure and roughness, but even more importantly presence of local adsorption sites of corrosion inhibitor at its low concentrations. The CPE impedance is given with eq. (5).

$$Z_{CPE} = [Q(j\omega)^{\alpha}]^{-1} \quad (5)$$

It should be noted that in the boundary case if $\alpha = 1$ the CPE impedance responds to capacitor of capacitance Q. Therefore CPE exponent α is often considered as the homogeneity factor, its decrease represents the increase of surface heterogeneity, while Q reflects the *quasi*-capacitance of the heterogeneous electrode. Furthermore, the CPE can be used to estimate the effective capacitance of studied electrode C_{eff}, with the use of Hirschorn's approximation for the surface distribution of the capacitance dispersion **[47]**:

$$C_{eff} = Q^{1/\alpha}\left(\frac{R_e R_{ct}}{R_e + R_{ct}}\right)^{(1-\alpha)/\alpha} \quad (6)$$

where R_e is resistance of the electrolyte and R_{ct} is charge transfer resistance.

The shift in calculated value of charge transfer resistance R_{ct} may be utilized to estimate the inhibition efficiency IE%, using the well-known relationship (7) **[15]**:

$$IE_{\%} = \left(1 - \frac{R_{ct}^{0}}{R_{ct}}\right) \quad (7)$$

where R_{ct}^{0} denounces the measured value of charge transfer resistance in the absence of the inhibitor. The results of impedance data analysis with the R(QR) EEC are summarized in Table 1.

Table 1 – Electric parameters of studied systems obtained from EIS results fitted with R(QR) EEC.

	buffer	*resorcinol*			*catechol*			*quinol*		
C_{inh} / mM	--	1	10	100	1	10	100	1	10	100
Q / $\mu Ss^{\alpha} \cdot cm^{-2}$	23.9	22	29.4	14.5	24.2	31.1	19	25.5	28	14.5
α / -	0.94	0.94	0.92	0.94	0.91	0.89	0.9	0.93	0.93	0.96
C_{eff} / $\mu F \cdot cm^{-2}$	10.7	10	10.8	8.2	7.5	7.6	6.5	10.7	11.8	9.4
R_{ct} / $k\Omega \cdot cm^{2}$	0.14	0.18	0.3	10.93	0.29	0.38	3.64	0.39	0.35	2.45
$IE_{\%}$ / %	--	22.2	53.3	98.7	51.7	63.2	96.2	64.1	60	94.3

Interestingly enough, the addition of resorcinol at the lowest concentration (1 mM) was providnig the lowest level of corrosion resistance. This feature most likely originates from the altered mechanism of molecules adsorption on the surface of aluminium alloy and was an object of further studies. On the other hand, presence of catechol and quinol offers approx. 60% efficiency already at c_{inh} = 1 mM, which does not significantly improve until reaching substantially higher concentrations. This may be observed in particular through effective capacitance C_{eff} changes, which decreased by nearly 30% already at the lowest inhibitor concentrations, compared to reference buffer electrolyte. The most important factor affecting this parameter is the thickness of the adsorbed layer on aluminium surface **[16]**.

Importantly, the highest inhibition efficiency was obtained after addition 100 mM of resorcinol. While the difference between IE% at this concentration does not exceed 4%, it should be noted that it corresponds to over 3x and nearly 5x higher R_{ct} values of AA5754 alloy in presence of resorcinol versus catechol and quinol, respectively. The increased efficiency of resorcinol at very high inhibitor concentrations was previously revealed in gravimetric studies **[48]**. In our opinion, its positive interaction is directly connected to the competitive formation of the corrosion products layer, making an additional barrier to aggressive environment. In the case of catechol and quinol, the barrier properties of the corrosion products layer are less evident, as discussed later.

3.2. The adsorbed layer chemistry

Authors decided to focus the core of electrochemical and physic-chemical studies on resorcinol and catechol isomers, which is due to nearly identical response and adsorption mechanism between catechol and quinol. At the same time, there is a significant solubility difference between these two compounds in aqueous electrolytes at 25 °C, hindering possible utilization of quinol as corrosion inhibitor. The solubility of quinol in 100g of water is 5.9 g versus 43 g for catechol and 110 g for resorcinol **[49]**.

The chemistry of the adsorbed dihydroxybenzene layer and corrosion products layer on the surface of studied aluminium alloy 5754 was evaluated with the use of high-resolution XPS analysis. First, samples were pre-exposed to alkaline electrolyte with the addition of studied inhibitor at 10 or 100 mM concentration for the period of 24 h. The XPS spectra in the binding energy (BE) range of *C1s*, *O1s*, *Al2p* and *Mg1s* peaks were collected and deconvoluted using below described fitting procedure. The results of the aforementioned deconvolution are summarized in Table 2.

Figure 4a presents the XPS spectra obtained in *Al2p* BE range. There is a clear shift in the peak position recorded between resorcinol-exposed and catechol-exposed aluminium samples. First, in

Peer-reviewed version available at Materials 2019, 12, 3067; doi:10.3390/ma12193067

the case of resorcinol, the primary peak doublet is located at higher BE values, with *Al2p*$_{3/2}$ peak at approx. 86.7 eV. This component was labelled Al_{ox2} and ascribed to the non-stoichiometry aluminium corrosion product layer, often observed in studies of this metal in pH range 10-12 **[50]**. The second component (Al_{ox1}), corresponding to native Al_2O_3 passive film was shifted at -1.9 eV. The presence of native oxide film results from air exposure of samples. The share of native oxides was nearly 5x smaller than this of non-stoichiometric oxides regardless of applied resorcinol concentration, suggesting that it is the presence of corrosion products layer which contributes the decrease of aluminium corrosion rate in resorcinol-exposed electrolytes.

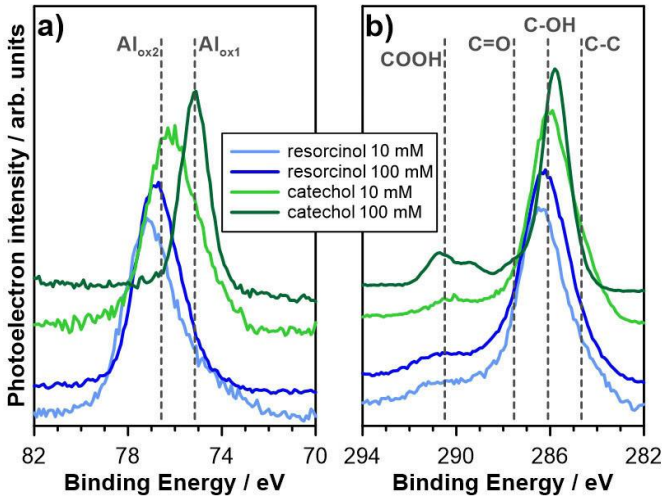

Fig. 4 – High-resolution XPS spectra recorded in a) *Al2p* and b) *C1s* binding energy range for aluminium alloy 5754 after 24 h exposure in bicarbonate buffer (pH = 11) with the addition of resorcinol or catechol at concentrations 10 and 100 mM.

On the other hand, addition of catechol at c_{inh} = 10 mM resulted in Al_{ox1}:Al_{ox2} share of 3.1:1.0. Significantly lower contribution from Al_{ox2} may suggest that presence of catechol contributes to the increased solubility of corrosion products at aluminium alloy 5754 surface. This observation was confirmed for higher concentration of catechol, where *Al2p* signal is composed solely from native oxide film.

The *C1s* spectra reveal significant presence of carbon species for both analyzed dihydroxybenzenes and at both concentrations, suggesting that inhibitor molecules indeed take part in formation of the adsorbed layer on aluminium alloy 5754 surface (Fig. 4b). The chemistry of this carbon species is strongly altered, however. In the case of catechol the amount of C-C and C-OH species, based on peaks at 284.7 and 286.0 eV respectively is nearly 3x compared to resorcinol at same concentrations **[51–53]**. Furthermore, the *C1s* spectra reveals significantly higher amount of carbonyl and/or carboxyl species for catechol-containing electrolyte (at BE exceeding 287.6 eV). These results corroborate previous findings regarding possible formation of the adsorbed inhibitor layer directly on aluminium surface and negligible participation of the corrosion products layer.

The *O1s* spectra deconvolution is in good accordance with previously discussed results. For the resorcinol-containing electrolyte, nearly 40 at.% of aluminium surface consists of oxygen atoms, with peak binding energies characteristic either for aluminium metal oxides (531.3 eV) or hydroxides (531.6 eV) **[15,16]**. However, in presence of catechol the amount of O^{2-} species is 2x lower at c_{inh} = 10 mM and 6.5x lower at 100 mM. Here, the signal corresponding from peaks located at approx. 532.6 eV is still strong, but rather of organic C-O interaction origin. The last deconvoluted *O1s* component is located at binding energies exceeding 532.7 eV. Its source are adsorbed carboxyl species, but also chemisorbed water molecules **[54]**. The non-stoichiometric corrosion products layer reveals high hydration level, confirmed with SEM micrographies, therefore higher share of chemisorbed water on surface of resorcinol-exposed aluminium alloy 5754 is natural.

Table 2 – Surface chemical composition (in at.%) for AA5754 after 24 h exposure in bicarbonate buffer (pH = 11) with addition of resorcinol or catechol, based on high-resolution XPS analysis.

Chemical state		BE / eV	Resorcinol		Catechol	
			10 mM	100 mM	10 mM	100 mM
Al2p$_{3/2}$	Al_{ox1}	74.8	3.2	2.3	3.4	8.0
	Al_{ox2}	76.7	14.7	15.3	10.5	---
C1s	C-C	284.7	4.6	5.4	10.4	6.0
	C-OH	286.0	12.8	16.9	31.4	32.8
	C=O	287.6	7.6	5.1	3.9	6.1
	COOH	290.3	2.8	2.4	3.9	8.6
O1s	O^{2-}	531.3	20.0	22.1	12.6	3.4
	CO/OH	532.6	15.2	18.5	20.2	29.2
	C=O/H_2O	533.7	18.0	11.0	3.0	5.6
Mg1s	Mg_{ox}	1303.1	1.1	1.0	0.7	0.3

Finally, the amount of magnesiu, the primary alloying additive, was only slightly altered between various investigated electrolytes. In each case magnesium was found in the form of hydroxides with *Mg1s* peak BE at 1303.1 eV, its higher contribution for resorcinol testifies presence of magnesium oxides in the corrosion products layer, having a possible effect on the increased corrosion resistance **[55]**.

SEM micrographs shown on Fig. 5 reveal significant difference in occurrence of the corrosion process for both studied dihydroxybenzene derivatives. The addition of resorcinol does not affect significantly surface topography, when comparing to reference aluminium alloy sample in buffer electrolyte (Fig. 5a). The oxidation is primarily oriented around the alloy microsctructure, which can be confirmed through local dissolution of alloy matrix surrounding intermetallic particles **[55–57]**. These particles appear on the micrographs with bright color. Based on own studies and the literature survey discussed particles are primarily composed of aluminium and alloying additives of Fe, Cr and Mn – each cathodic in nature compared to metal matrix **[57,58]**. Furthermore dense network of cracks visible on Fig. 5a-c testifies high hydration level of adsorbed layer and corrosion products layer on the electrode surface.

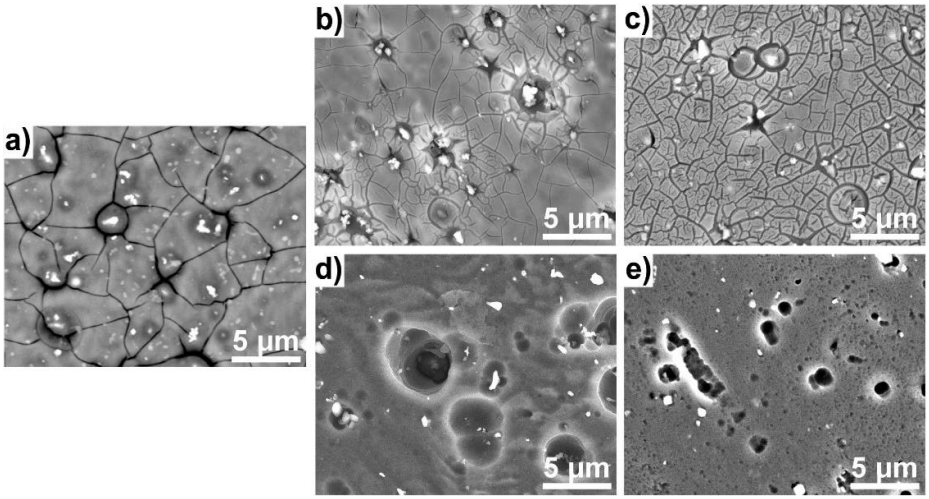

Fig. 5 – SEM micrographs of aluminium alloy 5754 surface exposed to bicarbonate buffer (pH = 11) for 24 h: a) in absence of corrosion inhibitor; with addition of resorcinol at concentration b) 10 mM and c) 100 mM or with addition of catechol d) 10 mM and e) 100 mM.

The presence of catechol or quinon in the electrolyte consequences in localized corrosion of aluminium, which is most often restricted to anodic Mg-rich phases and areas surrounding cathodic intermetallic particles. The absence of thick corrosion product layer effects in lack of cracks, which otherwise cover metal surface. The localized corrosion is naturally more evident at lower inhibitor

Peer-reviewed version available at Materials 2019, 12, 3067; doi:10.3390/ma12193067

concentrations (see Fig. 5d), where the spherical shape of caverns should be connected with local areas of hydrogen evolution in coupled cathodic reaction **[50].**

3.3. Thermodynamics of the adsorption process

The thermodynamics of dihydroxybenzene isomers adsorption was evaluated based on instantaneous impedance studies, carried out in galvanostatic mode (g-DEIS). Studied inhibitor is injected with linear injection rate (0.02 mL·min^{-1}), thus the instantaneous value of inhibitor concentration in the corrosion cell is known. Dynamic impedance measurements allows for a precise evaluation of the instantaneous values of electric parameters, where the inhibition efficiency may be estimated from R_{ct} using previously introduced eq. (7). Studies carried out in galvanostatic mode at $i_{DC} = 0$ ensures constant measurement conditions and lack of an additional polarization component, resulting from corrosion potential changes during inhibitor injection. The approach is characterized with higher accuracy, allowing to obtain larger data set and evaluate the exact inhibitor concentration at which the linear character of the adsorption isotherm is modified due to full electrode surface coverage with inhibitor monolayer. The details on the experimental procedure are presented elsewhere **[15,16]**.

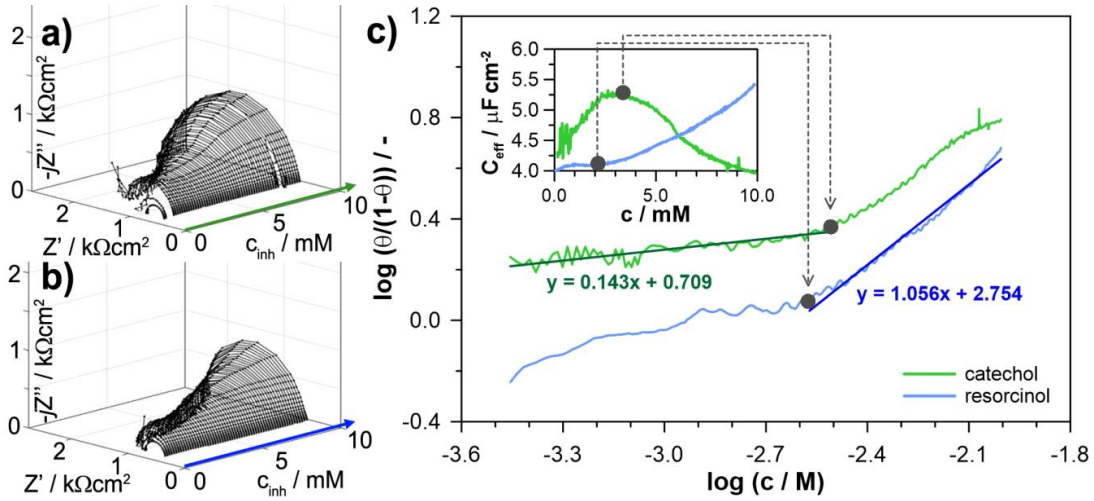

Fig. 6 – The g-DEIS impedance graphs of aluminium alloy 5754 in bicarbonate buffer (pH = 11), presented in Nyquist projection versus a) catechol and b) resorcinol concentration changes durnig its injection to corrosion cell. c) Langmuir model of adsorption isotherms drawn based on instantaneous R_{ct} changes, in the inset the instantaneous changes of effective capacitance C_{eff}.

The dynamic impedance spectra presented in the form of Nyquist plot are shown on Fig. 6a,b for resorcinol and catechol, respectively. The shape of the impedance spectra develops during corrosion inhibitor injection, where the increased impedance loop diameter testifies the increase of aluminium corrosion resistance. Fitting impedance spectra with R(QR) EEC allows for determination of dynamic changes of the electric parameters: R_{ct} and CPE within a timeframe of an analytical window length of a Short-Time Fourier Transform function, equal to 10 s in this case. The fitting procedure was carried out using dedicated software based on Nelder-Mead algorithm and build in LabView environment. Determination of the instantaneous R_{ct} values allowed for calculation of momentary inhibition efficiency IE%, which is also the measure of surface coverage with inhibitor molecules θ ($IE_{\%} = \theta * 100\%$). According to the principles of the most commonly used Langmuir adsorption isotherm, the adsorption equilibrium constant, K_{ads}, depends on surface coverage θ, which is given with eq. (8):

$$K_{ads} c_{inh} = \left(\frac{\theta}{1-\theta}\right) \quad (8)$$

In the linear range of eq. (8) the adsorption isotherm may serve for calculation of the adsorption Gibbs free energy ΔG, using eq. (9):

$$\Delta G = -RTln(K_{ads} * 55.5) \quad (9)$$

Peer-reviewed version available at *Materials* **2019**, *12*, 3067; doi:10.3390/ma12193067

Importantly, Langmuir isotherm conditions are only fulfilled for concentrations below full coverage with adsorbent monolayer. One should note, that classical approaches towards adsorption isotherm determination are based on merely few measurement points, where the non-linear behaviour resulting from aforementioned situation is difficult to track. On the other hand, the *quasi*-capacitance parameter obtained during g-DEIS impedance measurements allows to estimate the exact concentration required for monolayer formation by inhibitor molecules **[16]**.

Figure 6c presents the adsorption isotherms obtained with g-DEIS approach and plotted according to Langmuir model of molecules adsorption. The isotherms were drawn for resorcinol and catechol at concentrations in range 0-10 mM. It can be pointed out that both of these functions are characterized by loss of linear character and both have inflection at concentrations between 2 and 4 mM. However, the effective capacitance C_{eff} measurements plotted in the inset of Fig. 6c reveal significant differences in the adsorption mechanism.

There are three primary factors affecting value of capacitance according to eq. (10), namely: electrochemically active surface area A, permittivity ε and layer thickness d:

$$C = \frac{\varepsilon_0 \varepsilon A}{d} \quad (10)$$

where ε_0 is vacuum permittivity. Normalization of heterogeneity factor affecting *quasi*-capacitance Q and estimation of the effective capacitance C_{eff} allows to ignore the effect of electrode heterogeneity. Previous studies shown that with relatively short measurement duration the key factor influencing instantaneous C_{eff} of the adsorbed layer is its thickness **[16,35]**.

In the case of catechol-exposed AA5754 electrode, the C_{eff} value increases until reaching its maximum at c_{inh} = 3.5 mM and then decreases. Therefore, it should be assumed that the full coverage of aluminium surface with corrosion inhibitor molecules occurs at this concentration and the following C_{eff} decrease results from the increase in adsorbed layer thickness. The adsorption isotherm still remains linear afterwards, but no longer following the aforementioned restriction regarding surface coverage.

The situation is essentially different in the case of resorcinol-exposed AA5754 electrodes, where according to classic EIS and XPS studies the inhibitory action is generally lower. In the whole studied concentration range up to 10 mM the C_{eff} value effectively increases. The competitive interaction of the corrosion products layer and the resorcinol adsorption layer may have its effect on difficulties in assessing the full coverage of the adsorption layer, but also influences layer permittivity. As a result, the adsorption isotherm for resorcinol was following Langmuir model of adsorption at significantly higher inhibitor concentrations than catechol. On the other hand, the estimated inhibitor efficiency at the lowest concentrations is negligible and thus hard to measure. A conclusion should be made that the applicability of the Langmuir adsorption isotherm model for catechol and resorcinol lies in different inhibitor concentration ranges.

Following eqs. (8) and (9), the calculated values of Gibbs free energy ΔG of the adsorption process are presented in Table 3. Their negative values in both cases confirms spontaneous adsorption of both studied dihydroxybenzene molecules on aluminium alloy 5754 surface. Nevertheless, significantly different ΔG values between resorcinol and catechol suggests altered adsorption mechanism.

The more negative Gibbs free energy values are typical in case of chemisorption and formation of chemical bonds between filled π-orbitals in the oxygen atoms and partially unoccupied π-orbitals in the d-block metals. This is the postulated adsorption mechanism of resorcinol. Naturally, the value of this thermodynamic parameter may be further influenced by reported presence of nonstoichiometric corrosion products layer. On the other hand, our previous studied on carboxylic acids revealed that the less negative free Gibbs energies corresponds not only to the electrostatic interaction of the physisorption process but also the ligand exchange model of adsorption, resulting in formation of coordination compounds at the metal interface **[15,16]**. This is the case of catechol

interaction. The lower efficiency of ligand formation by resorcinol and quinol originates from the molecule geometry.

Table 3 – The applicability range of Langmuir adsorption model and the obtained thermodynamic parameters for resorcinol and catechol.

Isomer	Langmuir model c_{inh} range / mM	Adsorption equilibrium constant K_{ads}	Gibbs free energy ΔG / kJmol^{-1}
catechol	< 3.5	1.39	-10.77
resorcinol	2 – 10	11.38	-15.98

3.4. The keto-enol tautomerism

During the long-term exposure tests authors observed changes in color of studied electrolyte over time, resorcinol in particular (see inset of Fig. 7). These changes are followed by alteration of the electrochemical characteristics over time. On the other hand, for catechol and quinol the long-term inhibition efficiency is significantly higher. The g-DEIS studies were carried out once more to track the exact changes in the electrochemical behavior of aluminium alloy 5754 during 24 h exposure. The results of the impedance monitoring are presented on Fig. 7.

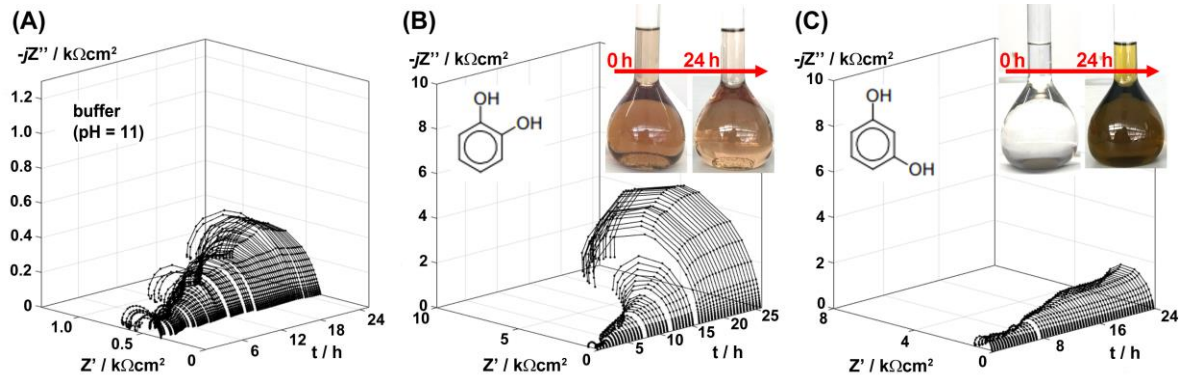

Fig. 7 – The g-DEIS impedance graphs of aluminium alloy 5754 in Nyquist projection during 24 h exposure in a) bicarbonate buffer (pH = 11) and with addition of: b) 10 mM catechol; c) 10 mM resorcinol

Analysis of the impedance data allows to bring the conclusion regarding long-term behavior of AA5754 in studied electrolytic conditions. Slight increase of the semicircle diameter over time, seen on the Nyquist projection for buffer-exposed sample, allows to conclude that the corrosion product layer forming on metal surface provides partial barrier properties and decrease the corrosion rate approximately 2.5x.

When expossed to buffer with addition of 10 mM catechol, the instantaneous charge transfer resistance is slightly higher (typically around 0.4 kΩ) and then gradually increases over time to reach significantly improved inhibition efficiency of ~98% after 24 h exposure. On the other hand, AA5754 exposed to electrolyte containing the same amount of resorcinol shows very small increase of charge transfer resistance over duration of the long-term exposure experiment.

The long-term exposure study allows to draw two important conclusions. First, there must be an additional interaction between studied inhibitor molecules and the electrolyte or the analyzed sample, which further differentiates the electrochemical characteristics of these dihydroxybenzene isomers over time. Second, when performing inhibitor efficiency measurements one has to take into consideration possible changes of investigated system characteristics. This is possible through carrying out fast measurements with techniques that allow non-stationary processes analyses (such as g-DEIS). Alternatively one should perform sufficiently long conditioning period, which might be different for each studied system. The latter approach, although more accessible, may cause problems with meeting conditions for many adsorption models.

Authors claim that the mechanism leading to further differentiation of adsorption by catechol and resorcinol on aluminium alloy surface is the keto-enol tautomerism, which may occur in aqueous alkaline environments. Nuclear magnetic resonance (NMR) studies were performed in order to verify this hypothesis.

^{1}H-NMR measurements have been performed in order to determine the presence of possible keto-enol forms in resorcinol in the alkaline conditions or to determine the formation of salt of those compounds. The studies of proton transfer by ^{1}H-NMR titration is usefull technique to determine the keto-enol equilibria **[59,60]**. The ^{1}H-NMR spectra of resorcinol dissolved in D_2O with addition of NaOH in molar ration of 1:5 and 1:10 are presented on Fig. 8. The ^{1}H-NMR spectra of resorcinol have been previously performed in D_2O **[61,62]**, while the titration of this compound by NaOH have not been investigated.

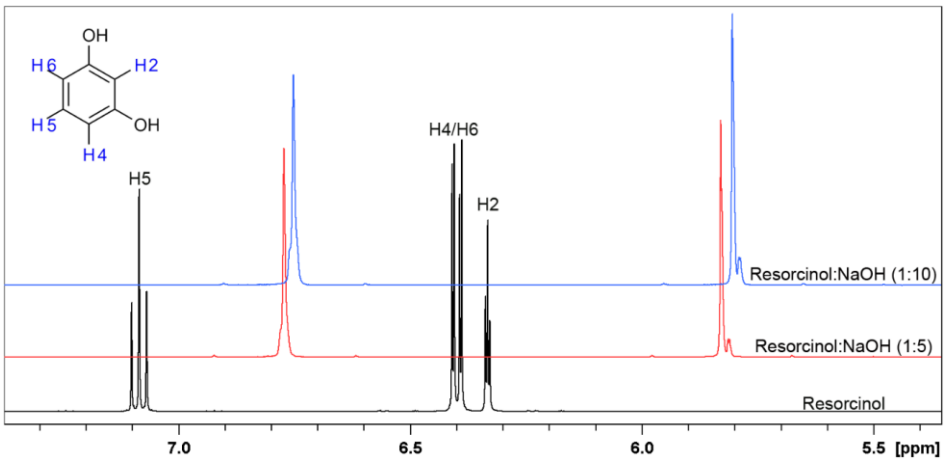

Fig. 8 - ^{1}H-NMR spectra of resorcinol in D_2O (black line) and in the presence of NaOH in D_2O in molar ratio 1:5 (red line) and 1:10 (blue line), respectively.

Two triplets are observed on spectra of resorcinol in D_2O, which correspond to H5 and H2, while two doublets correspond to H4 and H6. The spectra of resorcinol after addition of NaOH in molar ratio 1:5 changed diametrically. The shape, the chemical shifts and the multiplicity are different in comparison to the first one. Two main signals shifted towards negative values are now observed. This phenomenon indicates that the protons present in the structure of resorcinol are changed, further influencing the chemical shifts and the multiplicity. The addition of molar excess of NaOH in (1:10), does not cause any additional changes in ^{1}H-NMR spectrum shape, but the peaks are further shifted.

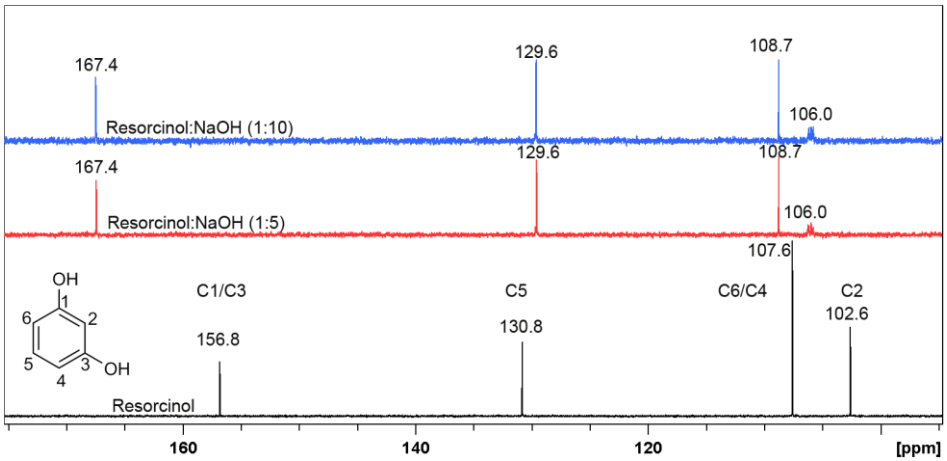

Fig. 9 - ^{13}C-NMR spectra of resircinol in D_2O (black line) and in the presence of NaOH in D_2O in molar ratio 1:5 (red line) and 1:10 (blue line), respectively.

The determination of new resorcinol derivative structure was possible after measuring the ^{13}C-NMR spectra, shown on Fig. 9. These spectra were performed in D_2O and after addition of

Peer-reviewed version available at Materials 2019, 12, 3067; doi:10.3390/ma12193067

NaOH in molar ratio 1:5 and 1:10, similar to previous experiment. It should be noticed that the peaks C4, C5, and C6 present in spectra before and after addition of NaOH does not change their position significantly. On the other hand peaks C1 and C3 overlapping at 156.8 ppm, change their position to 167.4 ppm with the addition of NaOH, which may indicate that keto form is present in the structure of resorcinol regardless the molar ratio. Additionally, after addition of NaOH the shift of peak C2 is obseved from 102.6 ppm to 106.0 ppm, this shift confirm the formation of keto form.

In the next step the ^{1}H-NMR and ^{13}C-NMR spectra were performed for catechol under the same experimental conditions. The ^{1}H-NMR spectra of catechol have been perfomed previously in aqueus solution, but under acidic pH = 2.4 **[63]** and in $CDCl_3$ **[64]**. The shape and chemical shifts of ^{1}H-NMR spectra illustrated on Fig. 10 are very similar to those in the literature.

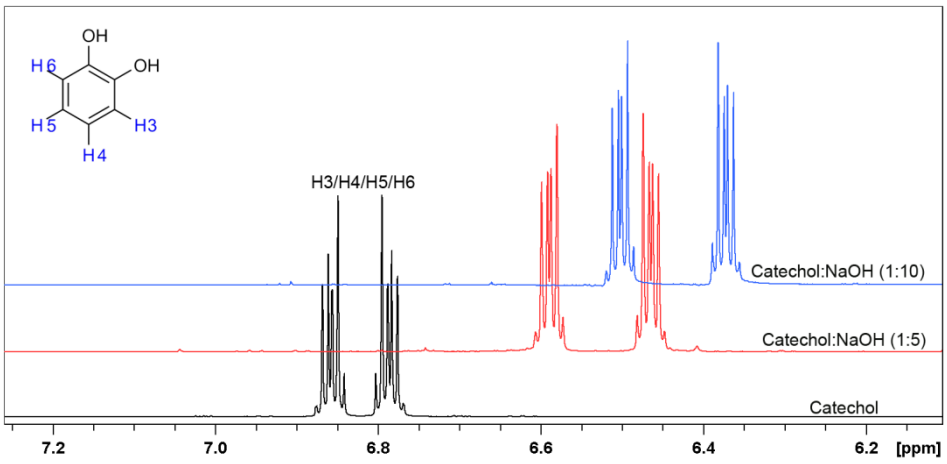

Fig. 10 - ^{1}H-NMR spectra of catechol in D_2O (black line) and in the presence of NaOH in D_2O in molar ratio 1:5 (red line) and 1:1 (blue line), respectively.

Two multiplets are present regardless of the solution, while the addition of NaOH in ratio 1:5 and 1:10, respectively, do not cause any changes in ^{1}H-NMR spectra shape, however, with increasing molar ratio of NaOH spectra are shifting towards more negative values. The above changes clearly indicate that the chemical structure of the catechol does not change significantly, while the shifts may indicate formation of sodium salts of catechol **[65]**.

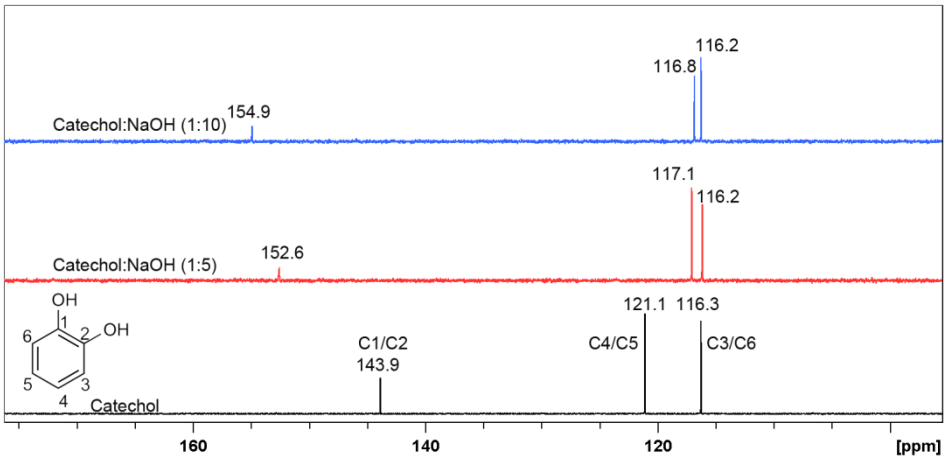

Fig. 11 - ^{13}C-NMR spectra of catechol in D_2O (black line) and in the presence of NaOH in D_2O in molar ratio 1:5 (red line) and 1:1 (blue line), respectively.

^{13}C-NMR spectra was performed in order to confirm formation of sodium salt of catechol in alkaline conditions, as shown on Fig. 11. Obtained data confirmed previously drawn assumption. ^{13}C-NMR spectra reveal ^{13}C chemical shifts for catechol in D_2O with the presence of NaOH in molar ratio 1:5 and 1:10. The C1 and C2 atoms connected to the hydroxyl groups in catechol in investigated solutions both give signal at 143.9 ppm in absence of NaOH, but after its addition signal is shifted towards 152.6 ppm and 154.9 ppm for ratio 1:5 and 1:10, respectively. The shift of carbon signals

directly indicate that catechol in alkaline solutions form a salt **[66]**. It is worth to notice that a small change of peak position was also observed for carbon C4/C5 and C3/C6 after additions of NaOH.

3.5. Dihydroxybenzene isomers adsorption mechanism

The overall interaction of the studied dihydroxybenzene isomers with aluminium alloy 5754 surface may thus be explained using the scheme presented on Fig. 12. Fig. 12a illustrates the case of aluminium corrosion in alkaline enviroments, according to the two-step mechanism discussed in the introduction section: 1) attack of OH^- ions on Al_2O_3 leading to its dissolution and $Al(OH)_3$ formation followed shortly-after by 2) chemical formation of $Al(OH)_4^-$ ions. The corrosion inhibition mechanism for catechol considers formation of ligands with aluminium ions (see Fig. 12b), which is hindered in case of resorcinol. On the other hand, resorcinol depends on formation of insoluble corrosion products layer, which to a large extent provides barrier mechanism towards corrosive electrolyte. The molecules chemisorb on the corrosion products layer, which becomes very efficient only at high inhibitor concentrations.

Lower inhibition efficiency of resorcinol at concentrations not exceeding 10 mM is connected with the keto-enol tautomerism mechanism, occuring in aqueous alkaline media and lowering the molecule influence on the corrosion protection (see Fig. 12c).

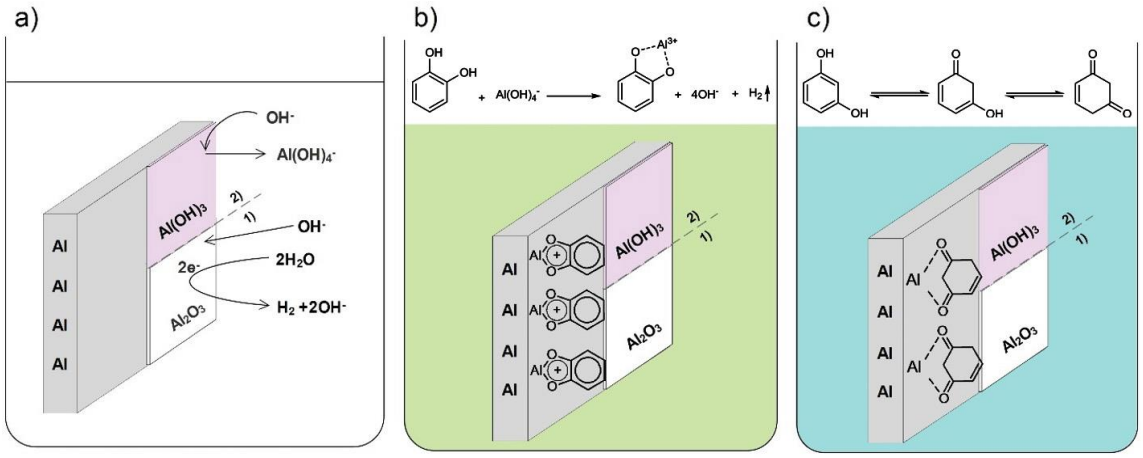

Fig. 12 – Schematic representation of aluminium corrosion mechanism in aqueous alkaline solutions: a) in absence of corrosion inhibitor and with addition of: b) catechol; c) resorcinol.

4. Conclusions

Understanding the interaction mechanism of inhibitor molecule with protected metal surface is of key importance in selection of the most efficient corrosion inhibitors, the most important in particular in case of green inhibitors based on natural extracts. While it is widely known how different functional groups affect the adsorption mechanism, the differences introduced by its location within the inhibitor molecule are often omitted.

In this study, we have revealed how location of hydroxyl groups affects the adsorption mechanism of dihydroxybenzene isomers and offered corrosion resistance toward aluminium alloy 5754 surface in alkaline environment. Utilization of Dynamic Electrochemical Impedance Spectroscopy in galvanostatic mode (g-DEIS) for adsorption isotherm determination allowed to confirm different forms of dihydroxybenzene interaction. All studied inhibitors followed the Langmuir model of adsorption, although we have observed that its applicability lies in different inhibitor concentration ranges.

Resorcinol was found to be characterized by the chemical adsorption mechanism. Its adsorption on aluminium surface is competitive to insoluble corrosion product layer formation, as shown with SEM and XPS studies. This interaction leads to the best inhibitor efficiency at the highest investigated concentration of 100 mM, but is not as efficient at lower concentrations. On the other

hand, catechol and quinol follows the ligand exchange model of adsorption. This leads to more efficient adsorption and increase corrosion protection even at lower corrosion concentrations: 1 and 10 mM. The adsorption process dominates insoluble corrosion product layer formation, which presence on analyzed surface was negligible.

The next significant difference lies in the long-term behavior and corrosion protection offered by dihydroxybenzene isomers in alkaline electrolyte. We have reported that resorcinol molecules undergo keto-enol tautomerism in sodium hydroxide solution, while the aforementioned process was negligible in the case of quinol and catechol. The tautomerism leads to rebuilding of the inhibitor molecule, electrolyte discoloration, but does not have significant influence on chemical adsorption mechanism by resorcinol over longer periods of time. It is even possible, that the presence of keto-enol tautomerism itself is the reason behind hindered adsorption of resorcinol and offered corrosion resistance. Keto forms were not observed in the structure of catechol and quinol molecules. At the same time their ability to complex metal ions leads to formation of layers with higher barrier properties and increased corrosion inhibition.

Author Contributions: conceptualization, J.R.; methodology, J.R. and J.W.; investigation, M.B., M.K., W.L. (electrochemical studies, SEM), J.R. (XPS) and P.N. (NMR); resources, J.R.; writing—original draft preparation, J.R., P.N., J.W. and W.L.; writing—review and editing, J.R. and J.W.; funding acquisition, J.R.

Funding: Authors acknowledge the financial support of the Polish Ministry of Science and Higher Education from the budget funds in the period 2016-2019 under Iuventus Plus project IP2015 067574.

Acknowledgments: Authors acknowledge Prof. Pawel Slepski and Prof. Artur Zielinski from Gdansk University of Technology for development of the software dedicated to effective DEIS data collection and analysis.

Conflicts of Interest: The authors declare no conflict of interest

References

1. Greenwood, N.N.; Earnshaw, A. *Chemistry of the elements*; 2nd ed.; Butterworth-Heinemann: Oxford ; Boston, 1997; ISBN 978-0-7506-3365-9.
2. Sanders, R.E.; Updated by Staff Aluminum and Aluminum Alloys. In *Kirk-Othmer Encyclopedia of Chemical Technology*; John Wiley & Sons, Inc., Ed.; John Wiley & Sons, Inc.: Hoboken, NJ, USA, 2012; p. 0112211319200112.a01.pub3 ISBN 978-0-471-23896-6.
3. Macdonald, D.D. Evaluation of Alloy Anodes for Aluminum-Air Batteries. *Journal of The Electrochemical Society* **1988**, *135*, 2410.
4. Chu, D.; Savinell, R.F. Experimental data on aluminum dissolution in KOH electrolytes. *Electrochimica Acta* **1991**, *36*, 1631–1638.
5. Pyun, S.-I.; Moon, S.-M. Corrosion mechanism of pure aluminium in aqueous alkaline solution. *Journal of Solid State Electrochemistry* **2000**, *4*, 267–272.
6. Armstrong, R.D.; Braham, V.J. The mechanism of aluminium corrosion in alkaline solutions. *Corrosion Science* **1996**, *38*, 1463–1471.
7. Li, Q.; Bjerrum, N.J. Aluminum as anode for energy storage and conversion: a review. *Journal of Power Sources* **2002**, *110*, 1–10.
8. Liu, Y.; Sun, Q.; Li, W.; Adair, K.R.; Li, J.; Sun, X. A comprehensive review on recent progress in aluminum–air batteries. *Green Energy & Environment* **2017**, *2*, 246–277.
9. Yang, S. Design and analysis of aluminum/air battery system for electric vehicles. *Journal of Power Sources* **2002**, *112*, 162–173.

10. Zhang, X.; Yang, S.H.; Knickle, H. Novel operation and control of an electric vehicle aluminum/air battery system. *Journal of Power Sources* **2004**, *128*, 331–342.
11. Singh, A.; Ansari, K.; Quraishi, M.; Lgaz, H. Effect of Electron Donating Functional Groups on Corrosion Inhibition of J55 Steel in a Sweet Corrosive Environment: Experimental, Density Functional Theory, and Molecular Dynamic Simulation. *Materials* **2018**, *12*, 17.
12. Al-Suhybani, A.A.; Sultan, Y.H.; Hamid, W.A. Corrosion of aluminium in alkaline solutions. *Materialwissenschaft und Werkstofftechnik* **1991**, *22*, 301–307.
13. Ebenso, E.E.; Isabirye, D.A.; Eddy, N.O. Adsorption and Quantum Chemical Studies on the Inhibition Potentials of Some Thiosemicarbazides for the Corrosion of Mild Steel in Acidic Medium. *IJMS* **2010**, *11*, 2473–2498.
14. Xhanari, K.; Finšgar, M. Organic corrosion inhibitors for aluminum and its alloys in chloride and alkaline solutions: A review. *Arabian Journal of Chemistry* **2016**.
15. Wysocka, J.; Krakowiak, S.; Ryl, J. Evaluation of citric acid corrosion inhibition efficiency and passivation kinetics for aluminium alloys in alkaline media by means of dynamic impedance monitoring. *Electrochimica Acta* **2017**, *258*, 1463–1475.
16. Wysocka, J.; Cieslik, M.; Krakowiak, S.; Ryl, J. Carboxylic acids as efficient corrosion inhibitors of aluminium alloys in alkaline media. *Electrochimica Acta* **2018**, *289*, 175–192.
17. Brito, P.S.D.; Sequeira, C.A.C. Organic Inhibitors of the Anode Self-Corrosion in Aluminum-Air Batteries. *Journal of Fuel Cell Science and Technology* **2013**, *11*, 011008.
18. Müller, B. Citric acid as corrosion inhibitor for aluminium pigment. *Corrosion Science* **2004**, *46*, 159–167.
19. Amin, M.A.; EI-Rehim, S.S.A.; El-Sherbini, E.E.F.; Hazzazi, O.A.; Abbas, M.N. Polyacrylic acid as a corrosion inhibitor for aluminium in weakly alkaline solutions. Part I: Weight loss, polarization, impedance EFM and EDX studies. *Corrosion Science* **2009**, *51*, 658–667.
20. Kumari, P.D.R.; Nayak, J.; Shetty, A.N. 3-Methyl-4-amino-5-mercapto-1,2,4-triazole as corrosion inhibitor for 6061 Al alloy in 0.5 M sodium hydroxide solution. *J Coat Technol Res* **2011**, *8*, 685–695.
21. Lashgari, M.; Malek, A.M. Fundamental studies of aluminum corrosion in acidic and basic environments: Theoretical predictions and experimental observations. *Electrochimica Acta* **2010**, *55*, 5253–5257.
22. Lashgari, M. Theoretical challenges in understanding the inhibition mechanism of aluminum corrosion in basic media in the presence of some p-phenol derivatives. *Electrochimica Acta* **2011**, *56*, 3322–3327.
23. Al-Amiery, A.; Al-Majedy, Y.; Kadhum, A.; Mohamad, A. New Coumarin Derivative as an Eco-Friendly Inhibitor of Corrosion of Mild Steel in Acid Medium. *Molecules* **2014**, *20*, 366–383.
24. Yang, W.; Wang, Q.; Xu, K.; Yin, Y.; Bao, H.; Li, X.; Niu, L.; Chen, S. Enhanced Corrosion Resistance of Carbon Steel in Hydrochloric Acid Solution by Eriobotrya Japonica Thunb. Leaf Extract: Electrochemical Study. *Materials* **2017**, *10*, 956.
25. Okeniyi, J.; Loto, C.; Popoola, A. Effects of Phyllanthus muellerianus Leaf-Extract on Steel-Reinforcement Corrosion in 3.5% NaCl-Immersed Concrete. *Metals* **2016**, *6*, 255.
26. Fares, M.M.; Maayta, A.K.; Al-Qudah, M.M. Pectin as promising green corrosion inhibitor of aluminum in hydrochloric acid solution. *Corrosion Science* **2012**, *60*, 112–117.
27. Abdel-Gaber, A.M.; Abd-El-Nabey, B.A.; Sidahmed, I.M.; El-Zayady, A.M.; Saadawy, M. Inhibitive action of some plant extracts on the corrosion of steel in acidic media. *Corrosion Science* **2006**, *48*, 2765–2779.

28. Abiola, O.K.; Otaigbe, J.O.E.; Kio, O.J. Gossipium hirsutum L. extracts as green corrosion inhibitor for aluminum in NaOH solution. *Corrosion Science* **2009**, *51*, 1879–1881.
29. Abiola, O.K.; Oforka, N.C.; Ebenso, E.E.; Nwinuka, N.M. Eco-friendly corrosion inhibitors: The inhibitive action of Delonix Regia extract for the corrosion of aluminium in acidic media. *Anti-Corrosion Methods and Materials* **2007**, *54*, 219–224.
30. Azzaoui, K.; Mejdoubi, E.; Jodeh, S.; Lamhamdi, A.; Rodriguez-Castellón, E.; Algarra, M.; Zarrouk, A.; Errich, A.; Salghi, R.; Lgaz, H. Eco friendly green inhibitor Gum Arabic (GA) for the corrosion control of mild steel in hydrochloric acid medium. *Corrosion Science* **2017**, *129*, 70–81.
31. de Souza, F.S.; Spinelli, A. Caffeic acid as a green corrosion inhibitor for mild steel. *Corrosion Science* **2009**, *51*, 642–649.
32. Abiola, O.K.; Otaigbe, J.O.E. The effects of Phyllanthus amarus extract on corrosion and kinetics of corrosion process of aluminum in alkaline solution. *Corrosion Science* **2009**, *51*, 2790–2793.
33. Singh, A.; Ahamad, I.; Quraishi, M.A. Piper longum extract as green corrosion inhibitor for aluminium in NaOH solution. *Arabian Journal of Chemistry* **2016**, *9*, S1584–S1589.
34. Abiola, O.K.; Otaigbe, J.O.E.; Kio, O.J. Gossipium hirsutum L. extracts as green corrosion inhibitor for aluminum in NaOH solution. *Corrosion Science* **2009**, *51*, 1879–1881.
35. Ryl, J.; Wysocka, J.; Cieslik, M.; Gerengi, H.; Ossowski, T.; Krakowiak, S.; Niedzialkowski, P. Understanding the origin of high corrosion inhibition efficiency of bee products towards aluminium alloys in alkaline environments. *Electrochimica Acta* **2019**, *304*, 263–274.
36. Talati, J.D.; Modi, R.M. O-Substituted Phenols as Corrosion Inhibitors for Aluminium-Copper Alloy in Sodium Hydroxide. *British Corrosion Journal* **1977**, *12*, 180–184.
37. Lakshmi, D.; Rajendran, S.; Sathiabama, J. Inhibition of Corrosion of Aluminium in Aqueous Solution at pH11 by Resorcinol-Zn2+ System. **2016**, 18.
38. Fouda, A.S.; Elasmy, A.A. Efficiency of some phenylthiosemicarbazide derivatives in retarding the dissolution of Al in NaOH solution. *Monatsh Chem* **1987**, *118*, 709–716.
39. Hassan, S.M.; Moussa, M.N.; El-Tagoury, M.M.; Radi, A.A. Aromatic acid derivatives as corrosion inhibitors for aluminium in acidic and alkaline solutions. *Anti-Corrosion Methods and Materials* **1990**, *37*, 8–11.
40. Obi-Egbedi, N.O.; Obot, I.B.; El-Khaiary, M.I. Quantum chemical investigation and statistical analysis of the relationship between corrosion inhibition efficiency and molecular structure of xanthene and its derivatives on mild steel in sulphuric acid. *Journal of Molecular Structure* **2011**, *1002*, 86–96.
41. Khaled, K.F. Electrochemical investigation and modeling of corrosion inhibition of aluminum in molar nitric acid using some sulphur-containing amines. *Corrosion Science* **2010**, *52*, 2905–2916.
42. Ramesh Babu, B.; Holze, R. Corrosion and hydrogen permeation inhibition for mild steel in HCl by isomers of organic compounds. *British Corrosion Journal* **2000**, *35*, 204–209.
43. Talati, J.D.; Desai, M.N.; Shah, N.K. Ortho-, meta-, and para-aminophenol-N-salicylidenes as corrosion inhibitors of zinc in sulfuric acid. *Anti-Corrosion Meth & Material* **2005**, *52*, 108–117.
44. Ryl, J.; Darowicki, K.; Slepski, P. Evaluation of cavitation erosion–corrosion degradation of mild steel by means of dynamic impedance spectroscopy in galvanostatic mode. *Corrosion Science* **2011**, *53*, 1873–1879.
45. Gerengi, H.; Darowicki, K.; Slepski, P.; Bereket, G.; Ryl, J. Investigation effect of benzotriazole on the corrosion of brass-MM55 alloy in artificial seawater by dynamic EIS. *Journal of Solid State Electrochemistry* **2010**, *14*, 897–902.

46. Gerengi, H. The Use of Dynamic Electrochemical Impedance Spectroscopy in Corrosion Inhibitor Studies. *Prot Met Phys Chem Surf* **2018**, *54*, 536–540.
47. Hirschorn, B.; Orazem, M.E.; Tribollet, B.; Vivier, V.; Frateur, I.; Musiani, M. Determination of effective capacitance and film thickness from constant-phase-element parameters. *Electrochimica Acta* **2010**, *55*, 6218–6227.
48. Talati, J.D.; Modi, R.M. Dihydroxy-benzenes as Corrosion Inhibitors for Aluminium—Copper Alloy in Sodium Hydroxide. *British Corrosion Journal* **1975**, *10*, 103–106.
49. Suresh, S.; Srivastava, V.C.; Mishra, I.M. Adsorption of catechol, resorcinol, hydroquinone, and their derivatives: a review. *Int J Energy Environ Eng* **2012**, *3*, 32.
50. Wysocka, J.; Krakowiak, S.; Ryl, J.; Darowicki, K. Investigation of the electrochemical behaviour of AA1050 aluminium alloy in aqueous alkaline solutions using Dynamic Electrochemical Impedance Spectroscopy. *Journal of Electroanalytical Chemistry* **2016**, *778*, 126–136.
51. Djordjevic, I.; Choudhury, N.R.; Dutta, N.K.; Kumar, S. Synthesis and characterization of novel citric acid-based polyester elastomers. *Polymer* **2009**, *50*, 1682–1691.
52. Amin, M.A.; Ahmed, E.M.; Mostafa, N.Y.; Alotibi, M.M.; Darabdhara, G.; Das, M.R.; Wysocka, J.; Ryl, J.; Abd El-Rehim, S.S. Aluminum Titania Nanoparticle Composites as Nonprecious Catalysts for Efficient Electrochemical Generation of H_2. *ACS Applied Materials & Interfaces* **2016**, *8*, 23655–23667.
53. Niedziałkowski, P.; Ossowski, T.; Zięba, P.; Cirocka, A.; Rochowski, P.; Pogorzelski, S.J.; Ryl, J.; Sobaszek, M.; Bogdanowicz, R. Poly-l-lysine-modified boron-doped diamond electrodes for the amperometric detection of nucleic acid bases. *Journal of Electroanalytical Chemistry* **2015**, *756*, 84–93.
54. McCafferty, E.; Wightman, J.P. Determination of the concentration of surface hydroxyl groups on metal oxide films by a quantitative XPS method. *Surface and Interface Analysis* **1998**, *26*, 549–564.
55. Ryl, J.; Wysocka, J.; Jarzynka, M.; Zielinski, A.; Orlikowski, J.; Darowicki, K. Effect of native air-formed oxidation on the corrosion behavior of AA 7075 aluminum alloys. *Corrosion Science* **2014**, *87*, 150–155.
56. Wloka, J.; Bürklin, G.; Virtanen, S. Influence of second phase particles on initial electrochemical properties of AA7010-T76. *Electrochimica Acta* **2007**, *53*, 2055–2059.
57. Yasakau, K.A.; Zheludkevich, M.L.; Lamaka, S.V.; Ferreira, M.G.S. Role of intermetallic phases in localized corrosion of AA5083. *Electrochimica Acta* **2007**, *52*, 7651–7659.
58. Goswami, R.; Spanos, G.; Pao, P.S.; Holtz, R.L. Precipitation behavior of the ß phase in Al-5083. *Materials Science and Engineering: A* **2010**, *527*, 1089–1095.
59. Novak, P.; Skare, D.; Sekusak, S. Substituent, temperature and solvent effects on keto-enol equilibrium in symmetrical pentane-1,3,5-triones. Nuclear magnetic resonance and theoretical studies. *Croatia Chemica Acta* **2000**, *73*, 1153–1170.
60. Billman, J.H.; Sojka, S.A.; Taylor, P.R. Investigations of keto–enol tautomerism by carbon-13 nuclear magnetic resonance spectroscopy. *J. Chem. Soc., Perkin Trans. 2* **1972**, 2034–2035.
61. Gaca, K.Z.; Parkinson, J.A.; Sefcik, J. Kinetics of early stages of resorcinol-formaldehyde polymerization investigated by solution-phase nuclear magnetic resonance spectroscopy. *Polymer* **2017**, *110*, 62–73.
62. Giles, R.; Kim, I.; Chao, W.E.; Moore, J.; Jung, K.W. Dual Studies on a Hydrogen–Deuterium Exchange of Resorcinol and the Subsequent Kinetic Isotope Effect. *J. Chem. Educ.* **2014**, *91*, 1220–1223.
63. Lambert, F.; Ellenberger, M.; Merlin, L.; Cohen, Y. NMR study of catechol and some catecholamines. *Org. Magn. Reson.* **1975**, *7*, 266–273.

64. Luisier, N.; Schenk, K.; Severin, K. A four-component organogel based on orthogonal chemical interactions. *Chem. Commun.* **2014**, *50*, 10233–10236.

65. Kim, H.; Gao, J.; Burgess, D.J. Evaluation of solvent effects on protonation using NMR spectroscopy: Implication in salt formation. *International Journal of Pharmaceutics* **2009**, *377*, 105–111.

66. Pretsch, E.; Buhlmann, P.; Badertscher, M. *Structure Determination of Organic Compounds*; Springer Berlin Heidelberg: Berlin, Heidelberg, 2009; ISBN 978-3-540-93809-5.